HHS Public Access

Author manuscript

*Int J Radiat Oncol Biol Phys*. Author manuscript; available in PMC 2017 November 01.

Published in final edited form as:

*Int J Radiat Oncol Biol Phys*. 2016 November 1; 96(3): 679–687. doi:10.1016/j.ijrobp.2016.06.2459.

# Evaluation of functional marrow irradiation based on skeletal marrow composition obtained using dual-energy CT

**Taiki Magome, PhD**[1,2,3], **Jerry Froelich, MD**[4], **Yutaka Takahashi, PhD**[2,5], **Luke Arentsen, PhD**[6], **Shernan Holtan, MD**[7], **Keenan Brown, PhD**[8], **Akihiro Haga, PhD**[3], **Keiichi Nakagawa, MD, PhD**[3], **Jennifer L. Holter Chakrabarty, MD**[9], **Sebastian Giebel, MD**[10], **Jeffrey Wong, MD**[11], **Kathryn Dusenbery, MD**[6], **Guy Storme, MD, PhD**[12], and **Susanta K Hui, PhD**[2,6,11]

[1]Department of Radiological Sciences, Faculty of Health Sciences, Komazawa University, Tokyo, Japan [2]Masonic Cancer Center, University of Minnesota, Minneapolis, Minnesota [3]Department of Radiology, The University of Tokyo Hospital, Tokyo, Japan [4]Department of Radiology, University of Minnesota, Minneapolis, Minnesota [5]Department of Radiation Oncology, Osaka University, Osaka, Japan [6]Department of Therapeutic Radiology, University of Minnesota, Minneapolis, Minnesota [7]Blood and Marrow Transplant Program, University of Minnesota, Minneapolis, Minnesota [8]Mindways Software Inc., Austin Texas [9]College of Medicine, Oklahoma Health Sciences Center [10]Department of Bone Marrow Transplantation, Comprehensive Cancer Center M. Curie-Sklodowska Memorial Institute, Branch Gliwice, Wybrzeze AK 15, Gliwice, Poland [11]Department of Radiation Oncology, Beckman Research Institute, City of Hope, Duarte, CA [12]Department of Radiotherapy, Universitair Ziekenhuis Brussel, Brussels, Belgium

## Abstract

**Purpose—**To develop an imaging method to characterize and map marrow composition in the entire skeletal system, and to simulate differential targeted marrow irradiation based on marrow composition.

**Methods and Materials—**Whole-body dual energy computed tomography (DECT) images of cadavers and leukemia patients were acquired, segmented to separate bone marrow components (namely; bone, red marrow (RM), and yellow marrow (YM)). DECT derived marrow fat fraction was validated using histology of lumbar vertebrae harvested from cadaver. Fraction of RM (RMF=RM/total marrow) and YMF were calculated in each skeletal region to assess correlation of marrow composition with sites and age. Treatment planning was simulated to target irradiation differentially at higher dose (18 Gy) to either RM or YM and lower dose (12 Gy) to rest of the skeleton.

Address for correspondence: Susanta K Hui, PhD, DABR, Department of Radiation Oncology and Beckman Research Institute, City of Hope, 1500 E Duarte Rd, CA 91010, shui@coh.org.

**Conflict-of-interest disclosure**: KB is a stockholder and employee of Mindways Software.

**Results—**A significant correlation between fat fractions obtained from DECT and cadaver histology samples was observed (r=0.861, p< 0.0001, Pearson). The RMF decreased in the head, neck and chest was significantly inversely correlated with age, but did not show any significant age-related changes in abdomen and pelvis regions. Conformity of radiation to targets (RM, YM) was significantly dependent on skeletal sites. The radiation exposure was significantly reduced (p< 0.05, t-test) to organs at risk (OARs) in RM and YM irradiation compared with standard total marrow irradiation (TMI).

**Conclusions—**Whole-body DECT offers a new imaging technique to visualize and measure skeletal-wide marrow composition. The DECT based treatment planning offers volumetric and site-specific precise radiation dosimetry of red and yellow marrow which varies with aging. Our proposed method could be used as a functional compartment of TMI for further targeted radiation to specific bone marrow environment, dose escalation, and/or reduction of doses to OARs.

### Keywords

Functional marrow; dual-energy CT; red marrow; yellow marrow; Total marrow irradiation

## INTRODUCTION

Total body irradiation (TBI) has been widely used for conditioning prior to hematopoietic cell transplantation (HCT). Dose escalation of TBI has produced decreased relapsed rates in patients with leukemia(1). However, treatment-related death also increased due to organ toxicity from TBI, thus negating any potential advantage for survival with escalated doses of TBI. Recently, total marrow irradiation (TMI) was developed, with clinical trials ongoing to achieve dose escalation with helical tomotherapy or volumetric modulated arc therapy (2–6) while reducing radiation dose to normal tissues. TMI focuses radiation to the entire skeleton, guided by whole body CT scan with the simplified assumption that hematologic disease is distributed homogeneously in the bone marrow. However, bone marrow is a complex physiological system with three primary components: (i) trabeculae rich (remodeling regions) osseous matrix, (ii) hematopoietically active red marrow (RM) (color due to hemoglobin in erythroid cells) that is highly vascularized (potentially well oxygenated and radiosenstive) with potential affinity of cancer cells for vascular endothelium, and (iii) yellow marrow (YM) (color due to carotenoids in fat droplets) with minimal hematopoiesis with paucity of vasculature (potentially low oxygen or hypoxic and radioresistant).

A recent pre-clinical study reported the existence of region-specific differences in development and regulation of marrow adipocytes with implications to understanding the marrow niche and skeletal metabolism (7). The pre-clinical study indicates the role of local bone marrow environment and survival of leukemia cells or leukemia resistance leading to treatment relapse (8–11). Similarly, the role of bone marrow microenvironment in multiple myeloma development is also reported (12). Following HCT, expanded adipocyte populations may negatively influence post-transplant hematopoietic engraftment (13). Moreover, cytotoxic conditioning regimen accelerate bone marrow damage delay in hematopoietic recovery and increase YM (14,15). The biopsy tool used to assess marrow, is limited to specific regions and lacks spatial resolution and the insertion of the needle probably damaged the local region, so that only an average reading was recorded. The water-

fat magnetic resonance imaging (WF-MRI) could differentiate marrow composition (16). However, it is inadequate for i) bone tissue imaging, ii) radiation dosimetric and planning purposes, iii) and whole body MRI will be prohibitively expensive and will require very long scan time. Despite growing appreciation of the bone marrow environment, it has remained clinically challenging to develop low cost, fast, whole body bone and marrow imaging for diagnostic and therapeutic purposes.

Here we report a novel development of whole body dual energy CT (DECT). The goals of this study were threefold: i) report pre-clinical validation of DECT predicting marrow fat (MF) simulation in physical space and correlating with histology in cadavers, ii) implement the DECT procedure to map 3D distribution of marrow composition in patients, and iii) simulate radiation planning targeting the bone marrow components.

## METHODS AND METERIALS

### Patients and cadaver characteristics

This study was approved by the University Institutional Review Board (XXXXXXX). In this study, whole-body DECT images of 7 cadavers (mean age of 60 ± 12 years old, 7 females) and 6 leukemia patients (mean age of 23 ± 17 years old, 5 males, 1 female) were acquired. Seven cadavers (died of progression of various cancer, underwent chemo-radiation treatment) were scanned DECT (140 and 80 kVp energy) (Somatom Definition Flash, Siemens, Germany) within 24 hours postmortem. Six patients were scanned for DECT (140 and the lowest available 90 kVp energy) (Brilliance Big Bore, Philips, Netherlands) as treatment planning CTs for total marrow irradiation (TMI). Each CT slice had a matrix size of 512 × 512, a slice thickness of 5.0 mm, a pixel size of 0.98–1.37 mm. Note that the Philips scanner uses sequential scans with two different energies, and the Siemens scanner uses a dual source. For the Philips scanner, two sequential scans were performed within a minute, and we assumed the sequential images were spatially overlapping. This assumption should be reasonable when imaging motionless phantoms and cadaveric specimen, but may present technical challenges when patient motion is feasible during imaging. As such, a dual energy CT scanner, which can scan with two different energies at one time, is preferred for the calculation of RM and YM in patients. The correlation between two scanners used in this study was checked by scanning QCT Pro phantom (Mindways Software, Austin, TX, USA), 50 ml tube filled with water, and intralipid 20% fat emulsion (Fresenius Kabi, Uppsala, Sweden). The correlation coefficient between two scanners was 0.998 ($p<0.0001$, Pearson). The detailed results were shown in supplement figure S1.

### Calculation of red and yellow marrow regions based on DECT

The upper body was divided into main four regions: head and neck (H&N), chest, abdomen, and pelvis regions (Figure 1) primarily considering a) skeletal regions with unique structures and nearby critical organs, b) change in radiation dose coverage to critical organs, when targeted radiation to adjacent bone marrow composition because of helical radiation delivery. For example, lung dose will be affected by the radiation delivery in skeletal system in chest regions.

A RM&YM composition image was calculated from DECT (two CT images with different energies) using a basis material composition method developed by Mindways for use with QCT Pro (Mindways Software, Austin, TX, USA). Details of this method were reported previously (16,17). Briefly, differences in HU estimates acquired at different x-ray energies are used to infer basis material composition ($H_2O$, $K_2HPO_4$) for each voxel in the spatially registered CT data sets. Resulting basis material compositions are interpreted relative to theoretical predictions of RM and YM basis material compositions obtained from energy-dependent mass attenuation coefficient and atomic composition data for published estimates of the typical composition of red and yellow marrow. Hence, basis material composition data is transformed to an RM&YM composition image. In the RM&YM composition image, a voxel with high RM component has high value, and a voxel with high YM component has low (negative) value. Therefore, red and yellow marrow regions can be separated within the total marrow regions by a threshold technique on the RM&YM composition image. First, total marrow regions (i.e., bone minus cortical bone regions) were manually contoured. Then, RM and YM regions were automatically segmented by threshold technique in total marrow regions; RM was defined as the voxels ≥ threshold value, and rest of the marrow was identified as YM. The optimal threshold value was determined from cadaver data by comparison of fat (YM) fraction obtained from DECT and histology samples (Figure 2a & b). The total of twenty-one lumbar vertebrae samples in 5 cadavers (4–5 samples/subject) were excised after performing DECT. Samples were decalcified, paraffin embedded, and stained with hematoxylin and eosin (H&E). The fat fraction was calculated as a ratio of fat volume per tissue volume within the intraosseal vertebral marrow space. Taking a histologic section from the center of the vertebral body ensured that the fat fraction was taken from a representative section of the imaging region of interest. The impact of CT scan slice thickness, skeletal sites, patient size on marrow fat estimation were examined using CIRS abdomen phantom (CIRS Inc, Norfolk, VA) and presented in supplement figure S2, S3, and S4.

## Simulation of red or yellow marrow irradiation

Radiation targeted to total marrow, RM, and YM are termed as TMI, RMI, and YMI respectively. The RMI and YMI plans were created in all 13 cases (7 cadavers and 6 patients) and compared with standard total marrow irradiation (TMI) plans. Upper body treatment planning (approximately 110 cm from head top to middle of femur) were created with Tomotherapy Planning Station (Accuray, Inc, Sunnyvale, CA, USA) for the irradiation with helical tomotherapy system (Accuray, Inc, Sunnyvale, CA, USA). For standard TMI, the entire skeleton (includes both red and yellow marrow) was used as a clinical target volume (CTV) and the planning target volume (PTV) was generated with 5 mm margin to CTV. The goal was to deliver 18 Gy to the PTV and minimize dose exposure to all critical organs, namely lungs, eyes, kidneys, liver, gut following recent reports (18,19). For differential targeted radiation, the PTV was separated into two groups: **i) RMI:** higher dose (18 Gy) irradiation to RM and lower dose (12 Gy) to rest of the skeletal system, and **ii) YMI:** 18 Gy irradiation to YM and 12 Gy to remaining skeleton. To compare PTV volume coverage of RM or YM relative to total marrow, we defined “PTVrm/PTVst”, “PTVym/PTVst” where PTVrm, PTVym, PTVst refers to PTV of RMI, YMI, and standard TMI, respectively. The prescription of 18 Gy in 6 fractions was used for planning simulation to

cover primary target with the 85% isodose line (18,19). The dose constraints for normal tissues were kept the same for each patient in order to keep median dose of all OARs < 10 Gy. Then, the priority of constraints for target dose uniformity was adjusted as high as possible. The field width, pitch, and modulation factor were set as 5mm (fixed), 0.2, and 2.5, respectively. The final dose distributions were calculated in fine mode grid space after 200 iterations of treatment planning optimization. Note that no additional times were needed for the optimization and calculation of dose distributions by incorporating RM or YM compared with standard TMI.

### Evaluation methodology

Segmented marrow regions were evaluated by red marrow fraction (RMF), which was calculated by the ratio of RM regions in total marrow regions. The RMF was calculated in each of the four regions (Figure 1). As a comparison of PTV doses, homogeneity index (HI) was calculated as follows:

$$HI = \frac{D5 - D95}{D_p} \times 100, \quad (1)$$

where, $D5$ and $D95$ is minimum dose in the PTV that encompasses at least 5% and 95% of the PTV, respectively, and $D_p$ is prescription dose. The primary target (prescribed 18 Gy) of each plan was used for the HI calculation. Hence, the PTVst, PTVrm, and PTVym were used for in standard TMI, RMI, and YMI, respectively. For organs at risk, mean dose and V10 (the percentage of the organ receiving ≥ 10 Gy) of lung, kidney, parotid, peritoneum were calculated. Student's paired t-tests (2 tails) were applied to compare dose indices between standard TMI and RMI or YMI. A correlation between two variables was calculated by Pearson product-moment correlation coefficient. A significant correlation was defined at the level of $p<0.05$ (2-tailed).

## RESULTS

### Verification of marrow fat

Figure 2a shows the sum of squared difference of fat fractions obtained from histology and DECT in cadaver data. From this result, the threshold value for the separation of RM and YM was set −45. Figure 2b shows relationship between fat fraction of histology and DECT with the threshold (−45). By using this threshold, correlation coefficient between fat fractions obtained from DECT and histology is 0.861 ($p< 0.0001$, Pearson). Figure 2b also shows the regression line between fat fraction of histology and DECT ($R^2 = 0.741$). The slope and intercept is 1.196 and −11.200, respectively. Independent 95% confidence intervals for the slope and intercept estimates are (0.856, 1.536) and (−24.812, 2.412), respectively.

### Measure and map marrow composition

As shown in Figure 3a there is a great anatomic variability of active marrow distribution among cases. As expected, the majority of marrow is active marrow in an 8 year old patient

(RMF = 97%), whereas a 54 year old patient has approximately half that value, 47% RMF. Figure 3b shows mean and standard deviation of regional RMF in 13 cases. Chest, abdomen, pelvis regions have relatively high mean RMF compared with H&N regions. Figure 3c shows relationships between RMF and patient age in 4 separate parts. There are significant correlations in H&N ($p<0.01$, Pearson) and chest ($p=0.01$, Pearson) regions, i.e., RMF decreases with age in these regions. The H&N region has relatively high negative correlation ($r = -0.778$) compared with chest regions ($r = -0.656$). There are no significant relationships between age and RMF in abdomen and pelvis regions ($p>0.05$, Pearson).

### Simulation of functional TMI

Next, we simulated differential radiation delivery and dose painting in which high dose may be focused towards red or yellow marrow and low dose to the remaining bone marrow. The PTVrm/PTVst & PTVym/PTVst were significantly ($p<0.001$, $p<0.001$, respectively, repeated measure one way ANOVA) different among 6 skeletal sites (Figure 4). As a representative case, Figure 5a shows dose painting of standard TMI, RMI, and YMI plans for the same subject, and Figure 5b shows corresponding dose volume histogram (DVH). The summary results of all patients are in Table 1. The HI of RMI and YMI were reduced significantly ($p<0.001$, $p<0.002$ respectively, paired t-test) compared to TMI. The HI is a signature of improving dose coverage. The significant dose (mean dose and V10) reduction were observed in RMI and YMI plan compared to TMI. When higher dose was given to either RM or YM (primary targets), we calculated dose reduction to the remaining skeletal sites (i.e, secondary target) (Table 1b). The average dose to secondary targets were significantly reduced for RMI planning (mean dose reduction, $p<0.001$, paired t-test) and YMI planning (mean dose reduction, $p<0.001$, paired t-test).

## DISCUSSION

TMI clinical studies adjusting dose continue to be examined extensively with the goal of improving the survival of patients with high-risk leukemia and other hematologic diseases by reducing both relapse and toxicity. Here we presented a novel methodology to map RM and YM using DECT throughout the skeleton, providing a new insight of site dependent changes of marrow composition with aging. DECT imaging guidance is expected to facilitate multi-target differential radiation delivery to the specific marrow compositions and reduces critical organ toxicity and preserve bone marrow.

The physiological validation of DECT imaging demonstrated that a modality already incorporated into radiation planning could be extended to measure YM fraction. A number of imaging studies have been published to estimate RM and YM (20–23). In a clinical study, we previously reported water-fat magnetic resonance imaging (WF-MRI) to visualize and map marrow compositions and its high correlation with DECT derived marrow fat measurements (16,24). Due to technical difficulties, lengthy scanning time, and cost, the use of WF-MRI is mainly confined to small skeletal regions. Diagnostic superiority of WF-MRI over CT may be aptly use to verify and spot check marrow composition certain regions, but it will not be practical as a modality for radiotherapy dose calculation secondary to time constraints. Whole body CT scanning is currently in clinical use for TMI treatment planning,

thus implementation of DECT in the clinic is logical and straightforward without additional cost or radiation burden. Several modern CT scanners are equipped with a dual energy CT method without additional scans or radiation exposure than single energy CT scans. In fact, the iterative reconstruction technology has further significantly reduced the radiation dose to patients and improved imaging quality of DECT. (25) Taken together, the DECT is economically viable and may find advantageous for assessment of skeletal composition and functional marrow irradiation.

The distribution of RM and YM (Figure 3) was the first observation in human through the skeletal system. Although, overall RM decreases and YM increases with age, RM remains active in certain skeletal sites (abdominal & pelvic regions) in older age defying common association between RM, YM & age (26). Also, the RMF in H&N region has higher negative correlation ($r = -0.778$) with age than the RMF in chest region ($r = -0.656$). Preclinical studies began to unravel the complex nature of bone marrow adipocyte development, skeletal region site differences, and potential roles in bone marrow niche, (7) and engraftment (13). YM or adipocytes have been shown to relate to disease resistance for multiple reasons: lower vascular system/higher hypoxic, saturated fatty acid composition. Saturated fat may function to enhance cancer resistance to systemic chemotherapy and radiation (27). The majority of the patients undergoing HCT receive prior chemotherapy treatment. Because cancer treatment changes marrow fat composition, (16) individual factors including age and prior treatment may influence the distribution of marrow composition in different sites. Thus, if treatment is developed for differential radiation delivery to individual marrow composition, it will have to be individualized ( personalized medicine). Escalated doses of targeted radiation to YM regions may provide a unique therapeutic benefit. Preclinical studies to measure radiosensitivity of leukemia in RM and YM should be conducted.

This study has several limitations which will be essential for future developments. First, previous cancer treatment could change the marrow composition of cadavers. Our goal was to use cadavers for pre-clinical validation of DECT predicting marrow fat simulation in physical space, validate with histology, and initiate TMI simulation, making it feasible for clinical translation. As well, all high risk/relapsed patients who undergo the TMI trial had prior chemotherapy treatment several years ago, which may impact their marrow composition. These groups may have different marrow distribution than healthy patients. However, this imaging could be seen as a strength of the study as it on understanding association between marrow adipose development and treatment resistance or relapse, and potentially allow target marrow compositions differentially. In future, FLT PET/DECT (3′-deoxy-3′[(18)F]-fluorothymidine) imaging could help assessing disease activity distribution (with potentially associated with higher relapse (28)) and association with marrow compositions. As the CT scan is part of PET-CT imaging, integration of this process will be easier and cost-effective. However, one may need to verify marrow composition with a gold standard MRI in some skeletal sites, as shown in our previous work (16). Second, although 18 Gy was prescribed to the primary target in this simulation, it is not clear how much dose and fraction should be prescribed for clinical practice. Clinical marrow irradiation dose finding studies must be completed to extend this to clinical use. Moreover, chemotherapy

may also affect dose sensitivity (6). Thus, one should carefully determine the suitable dose and dose per fraction.

The future diversification of current clinical TMI studies for differential targeting to RM and YM will most likely require clinical evidence. As well, the radiobiological effectiveness of a specific dose delivered to two different marrow compartments needs to be investigated. However, with current development, the use of DECT-based imaging would allow for retrospective calculation of doses delivered to particular BM compartments and its effect on the treatment efficacy. This could give a platform for second generation clinical trials with dose escalation on either RM or YM, dependent on previously achieved clinical data. Recent FDG-PET/CT indicates potential re-distribution of bone marrow after bone marrow transplant (29). The DECT with lower cost and reduced dose exposure, may be easily incorporated in patient management to measure Post-TMI/bone marrow transplant redistribution of marrow compositions and bone damage, similar to our recent report (16). The DECT imaging development may also be used for the diagnosis of lytic bone changes and the assessment of fracture risk in multiple myeloma (MM) similar to previously shown low-dose whole-body multidetector row-CT (MDCT). (30,31) The ability to distinguish bone and marrow composition may further provide a tool to assess the involvement and progression of MM in specific skeletal environment (marrow composition and bone). The assessment of fracture risk or BMD must be carefully evaluated when using conventional CT scan as our recent work shows post cancer treatment rapid increase in marrow fat component artificially reduce BMD more than actual changes in bone and thus DECT provides an additional tool to assess true change in BMD correcting for change in marrow fat. (16)

In conclusion, we developed a novel DECT-based imaging method to measure marrow composition and visualize skeletal wide 3D marrow composition. The DECT guided radiation treatment planning offers volumetric and site-specific radiation dosimetry of red and yellow marrow which varies with aging. Simulation reveals that the DECT guidance could allow functional marrow irradiation by delivering differential radiation treatment to specific marrow and bone compositions. The red or yellow marrow irradiation may also reduce critical organ toxicity and preserve bone marrow function.

## Supplementary Material

Refer to Web version on PubMed Central for supplementary material.

## Acknowledgments

This work was supported by National Institutes of Health grant 1R01CA154491-01, the Japan Society for the Promotion of Science (JSPS) Core-to-Core Program (No. 23003), Grant-in-Aid for JSPS Fellow (13J02944), and Grant-in-Aid for Young Scientists (B) (26860397).

## References

1. Clift RA, Buckner CD, Appelbaum FR, et al. Long-term follow-up of a randomized trial of two irradiation regimens for patients receiving allogeneic marrow transplants during first remission of acute myeloid leukemia. Blood. 1998; 92:1455–6. [PubMed: 9694737]
2. Hui SK, Kapatoes J, Fowler J, et al. Feasibility study of helical tomotherapy for total body or total marrow irradiation. Medical Physics. 2005; 32:3214. [PubMed: 16279075]

3. Schultheiss TE, Wong J, Liu A, et al. Image-guided total marrow and total lymphatic irradiation using helical tomotherapy. Int J Radiat Oncol Biol Phys. 2007; 67:1259–67. [PubMed: 17336225]
4. Aydogan B, Yeginer M, Kavak GO, et al. Total marrow irradiation with rapidarc volumetric arc therapy. Int J Radiat Oncol Biol Phys. 2011; 81:592–9. [PubMed: 21345619]
5. Corvo R, Zeverino M, Vagge S, et al. Helical tomotherapy targeting total bone marrow after total body irradiation for patients with relapsed acute leukemia undergoing an allogeneic stem cell transplant. Radiother Oncol. 2011; 98:382–6. [PubMed: 21339008]
6. Wong JY, Forman S, Somlo G, et al. Dose escalation of total marrow irradiation with concurrent chemotherapy in patients with advanced acute leukemia undergoing allogeneic hematopoietic cell transplantation. Int J Radiat Oncol Biol Phys. 2013; 85:148–56. [PubMed: 22592050]
7. Scheller EL, Doucette CR, Learman BS, et al. Region-specific variation in the properties of skeletal adipocytes reveals regulated and constitutive marrow adipose tissues. Nature communications. 2015:6.
8. Kode A, Manavalan JS, Mosialou I, et al. Leukaemogenesis induced by an activating beta-catenin mutation in osteoblasts. Nature. 2014; 506:240–4. [PubMed: 24429522]
9. Konopleva MY, Jordan CT. Leukemia stem cells and microenvironment: Biology and therapeutic targeting. Journal of clinical oncology: official journal of the American Society of Clinical Oncology. 2011; 29:591–9. [PubMed: 21220598]
10. Raaijmakers MH. Niche contributions to oncogenesis: Emerging concepts and implications for the hematopoietic system. Haematologica. 2011; 96:1041–8. [PubMed: 21459792]
11. Schepers K, Pietras EM, Reynaud D, et al. Myeloproliferative neoplasia remodels the endosteal bone marrow niche into a self-reinforcing leukemic niche. Cell stem cell. 2013; 13:285–99. [PubMed: 23850243]
12. Wang J, De Veirman K, De Beule N, et al. The bone marrow microenvironment enhances multiple myeloma progression by exosome-mediated activation of myeloid-derived suppressor cells. Oncotarget. 2015
13. Naveiras O, Nardi V, Wenzel PL, et al. Bone-marrow adipocytes as negative regulators of the haematopoietic microenvironment. Nature. 2009; 460:259–263. [PubMed: 19516257]
14. Wilke C, Holtan SG, Sharkey L, et al. Marrow damage and hematopoietic recovery following allogeneic bone marrow transplantation for acute leukemias: Effect of radiation dose and conditioning regimen. Radiother Oncol. 2015
15. Wang Y, Liu L, Pazhanisamy SK, et al. Total body irradiation causes residual bone marrow injury by induction of persistent oxidative stress in murine hematopoietic stem cells. Free radical biology & medicine. 2010; 48:348–56. [PubMed: 19925862]
16. Hui SK, Arentsen L, Sueblinvong T, et al. A phase i feasibility study of multi-modality imaging assessing rapid expansion of marrow fat and decreased bone mineral density in cancer patients. Bone. 2015; 73:90–97. [PubMed: 25536285]
17. Arentsen L, Yagi M, Takahashi Y, et al. Validation of marrow fat assessment using noninvasive imaging with histologic examination of human bone samples. Bone. 2015; 72:118–22. [PubMed: 25460181]
18. Hui SK, Verneris MR, Higgins P, et al. Helical tomotherapy targeting total bone marrow - first clinical experience at the university of minnesota. Acta Oncol. 2007; 46:250–5. [PubMed: 17453378]
19. Takahashi Y, Verneris MR, Dusenbery KE, et al. Peripheral dose heterogeneity due to the thread effect in total marrow irradiation with helical tomotherapy. International Journal of Radiation Oncology* Biology* Physics. 2013; 87:832–839.
20. Wyss JC, Carmona R, Karunamuni RA, et al. [(18)f]fluoro-2-deoxy-2-d-glucose versus 3′-deoxy-3′-[(18)f]fluorothymidine for defining hematopoietically active pelvic bone marrow in gynecologic patients. Radiother Oncol. 2016; 118:72–8. [PubMed: 26674924]
21. Carmona R, Pritz J, Bydder M, et al. Fat composition changes in bone marrow during chemotherapy and radiation therapy. International Journal of Radiation Oncology* Biology* Physics. 2014; 90:155–163.

22. Rose BS, Liang Y, Lau SK, et al. Correlation between radiation dose to (1)(8)f-fdg-pet defined active bone marrow subregions and acute hematologic toxicity in cervical cancer patients treated with chemoradiotherapy. Int J Radiat Oncol Biol Phys. 2012; 83:1185–91. [PubMed: 22270171]
23. Roeske JC, Lujan A, Reba RC, et al. Incorporation of spect bone marrow imaging into intensity modulated whole-pelvic radiation therapy treatment planning for gynecologic malignancies. Radiother Oncol. 2005; 77:11–7. [PubMed: 16024116]
24. Bolan PJ, Arentsen L, Sueblinvong T, et al. Water-fat mri for assessing changes in bone marrow composition due to radiation and chemotherapy in gynecologic cancer patients. Journal of magnetic resonance imaging: JMRI. 2013
25. Flohr T, McCollough C, Bruder H, et al. First performance evaluation of a dual-source ct (dsct) system. European Radiology. 2006; 16:256–268. [PubMed: 16341833]
26. Tuljapurkar SR, McGuire TR, Brusnahan SK, et al. Changes in human bone marrow fat content associated with changes in hematopoietic stem cell numbers and cytokine levels with aging. Journal of anatomy. 2011; 219:574–581. [PubMed: 21923862]
27. Conklin KA. Dietary polyunsaturated fatty acids: Impact on cancer chemotherapy and radiation. Alternative medicine review. 2002; 7:4–21. [PubMed: 11896743]
28. Vanderhoek M, Juckett MB, Perlman SB, et al. Early assessment of treatment response in patients with aml using [18f] flt pet imaging. Leukemia Research. 2011; 35:310–316. [PubMed: 20832860]
29. Fiz F, Marini C, Campi C, et al. Allogeneic cell transplant expands bone marrow distribution by colonizing previously abandoned areas: An fdg pet/ct analysis. Blood. 2015; 125:4095–102. [PubMed: 25957389]
30. Horger M, Claussen CD, Bross-Bach U, et al. Whole-body low-dose multidetector row-ct in the diagnosis of multiple myeloma: An alternative to conventional radiography. European journal of radiology. 2005; 54:289–297. [PubMed: 15837412]
31. Lecouvet FE, Berg BCV, Michaux L, et al. Development of vertebral fractures in patients with multiple myeloma: Does mri enable recognition of vertebrae that will collapse? Journal of computer assisted tomography. 1998; 22:430–436. [PubMed: 9606386]

## SUMMARY

Red and yellow marrow regions (RM or YM) were segmented from whole body dual-energy computed tomography (DECT) and dose escalations to specific marrow regions were simulated. While CT guided total marrow irradiation (TMI) delivers radiation to skeletal regions, the DECT-based imaging would allow precisely determine doses delivered to particular bone marrow compartments, its effect on the treatment efficacy, and provide a platform for second generation clinical trials with dose escalation on either RM or YM.

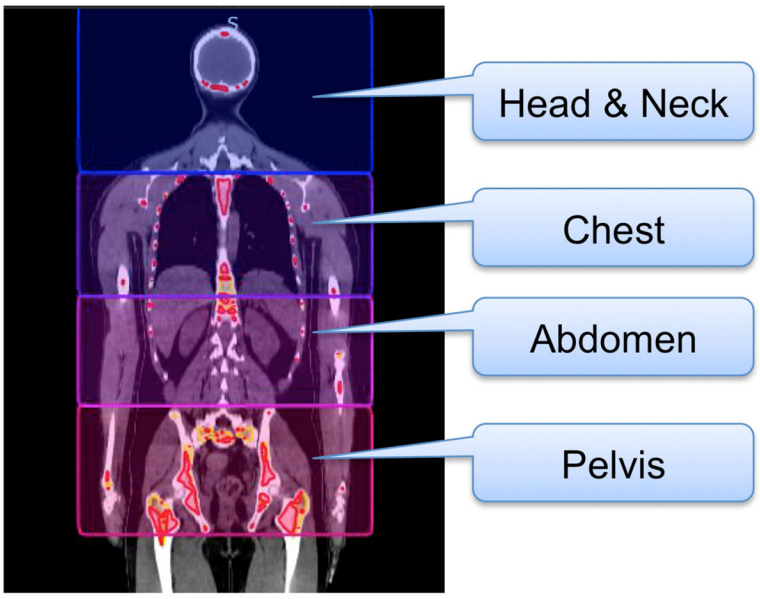


**Figure 1.**
Volume of interest of regional analysis, i.e., head and neck, chest, abdomen, and pelvis regions.

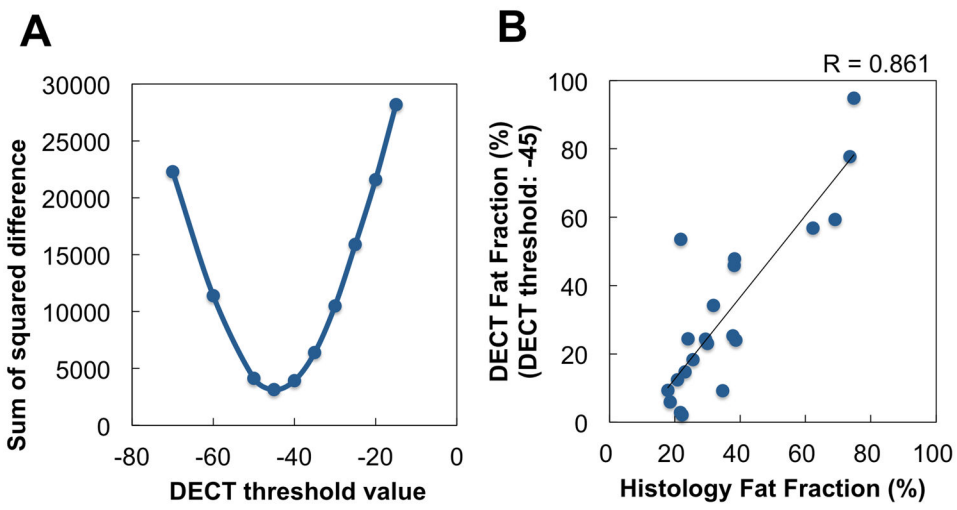


**Figure 2.**

Correlation between fat fractions obtained from dual-energy computed tomography and histology in cadaver data. (a) Relationship between DECT threshold and sum of squared difference of fat fractions obtained from histology and DECT. From this result, the threshold value for the separation of RM and YM was set −45. (b) Relationship between fat fraction of histology and DECT with the threshold value of −45.

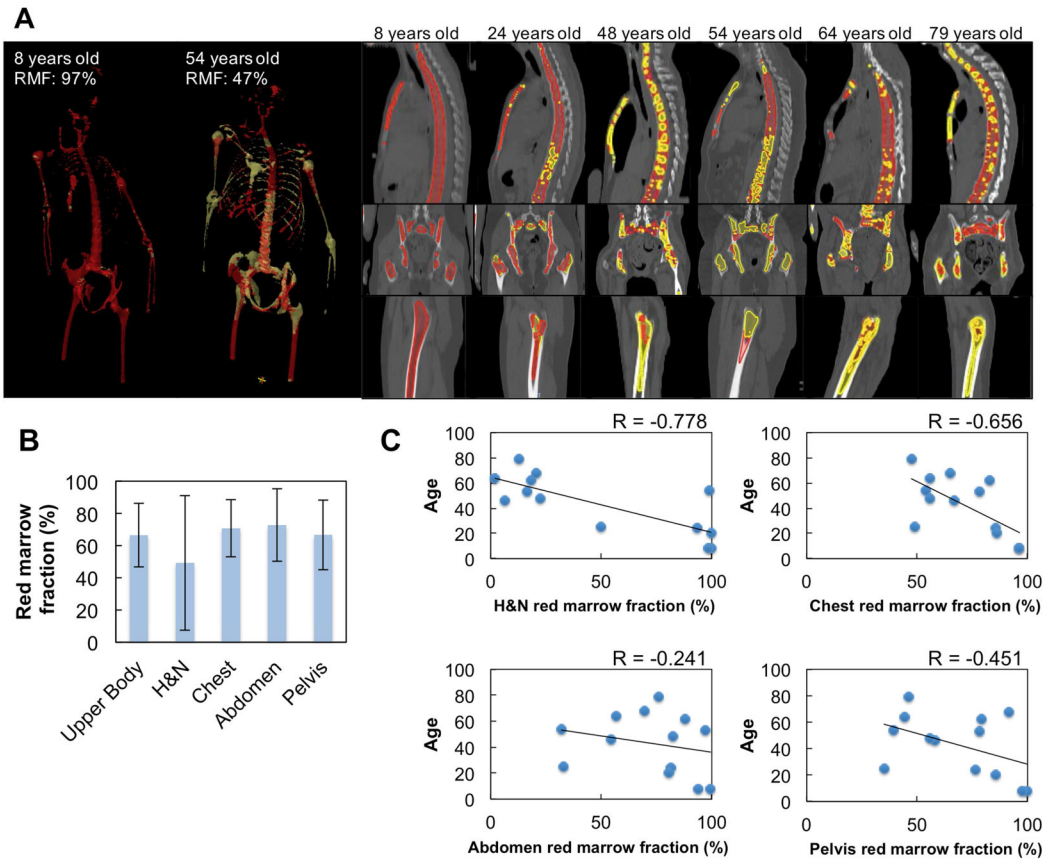


**Figure 3.**

Distribution of red marrow and marrow fat. (a) Representative marrow distribution of various patients and cadavers. Red regions show red marrow and yellow regions indicate yellow marrow. (b) Means and standard deviations of red marrow fractions in 13 cases. (c) relationship between red marrow fraction and age.

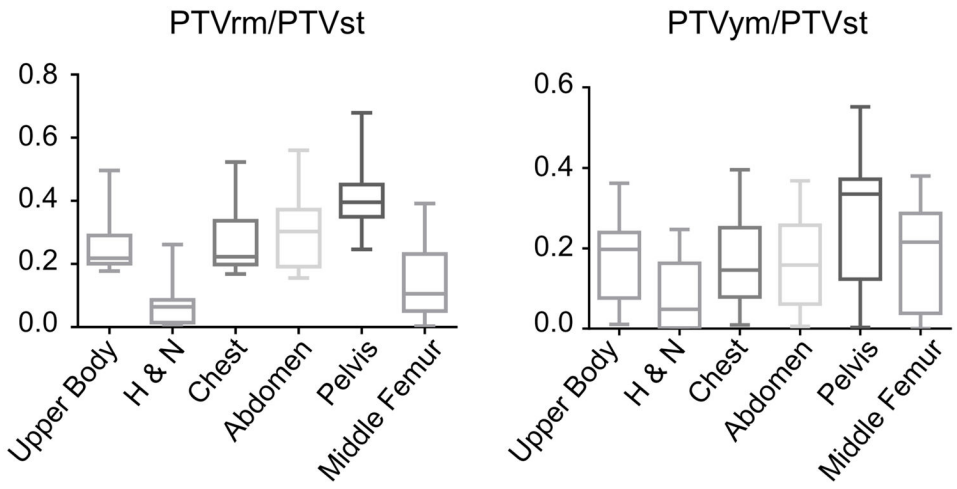


**Figure 4.**

Planning target volume coverage of red marrow or yellow marrow relative to total marrow. The coverages were significantly (<0.001, <0.001, respectively, repeated measure one way ANOVA) different among 6 skeletal sites.

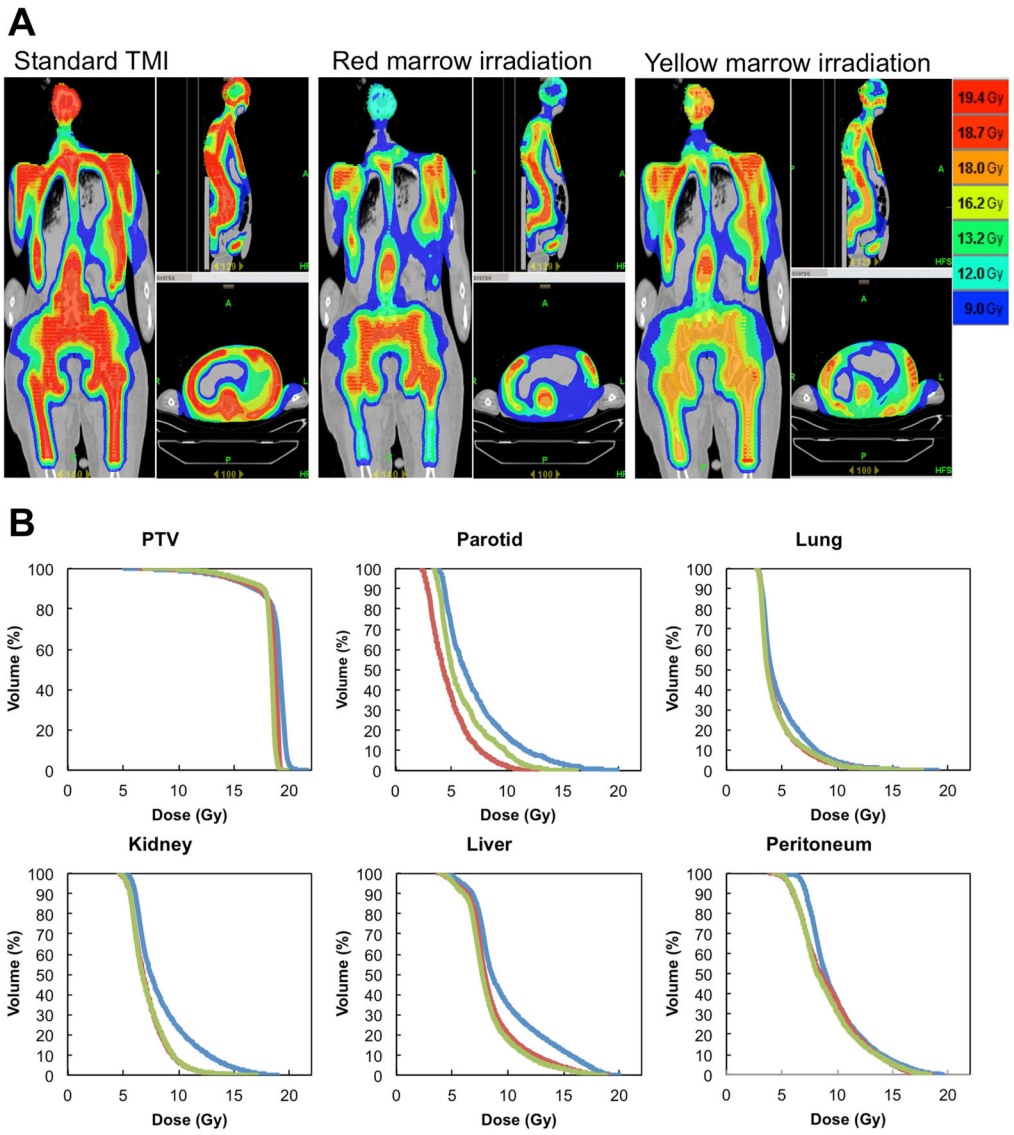


**Figure 5.**

Comparison of standard total marrow irradiation (TMI), red marrow irradiation (RMI), and yellow marrow irradiation (YMI). (a) Dose distributions of standard TMI, RMI, and YMI. (b) Dose volume histogram (DVH) for standard TMI, RMI, and YMI. blue, red, and green line indicate DVHs of standard TMI plan, RMI plan, and YMI plan respectively. Here, DVH of PTV shows primary target prescribed by 18 Gy, i.e., wholebone, red marrow, yellow marrow for standard TMI, RMI, YMI, respectively.

**Table 1**

Comparison of dose indices, (a) mean and standard deviation (SD) of dose indices between standard total marrow irradiation (StTMI), red marrow irradiation (RMI), and yellow marrow irradiation (YMI). Here, the primary target (prescribed 18 Gy) of each plan was used for the homogeneity index calculation. (b) mean dose comparison of primary targets and remaining skeletal sites (secondary targets) in red marrow irradiation and yellow marrow irradiation.

**A**

| | | Standard TMI mean ± SD | RMI mean ± SD | p value (StTMI vs. RMI) | YMI mean ± SD | p value (StTMI vs. YMI) | p value (RMI vs. YMI) |
|---|---|---|---|---|---|---|---|
| **PTV** | homogeneity index | 20.87 ± 3.42 | 14.14 ± 6.09 | 0.001 | 14.43 ± 5.49 | 0.002 | 0.873 |
| **lung** | mean dose (Gy) | 7.64 ± 2.13 | 7.37 ± 2.30 | 0.002 | 7.45 ± 2.54 | 0.171 | 0.581 |
| | V10 (%) | 23.49 ± 14.03 | 20.68 ± 13.60 | 0.006 | 20.29 ± 15.93 | 0.116 | 0.842 |
| **kidney** | mean dose (Gy) | 8.48 ± 0.37 | 7.76 ± 0.49 | < 0.0001 | 7.57 ± 0.46 | < 0.0001 | 0.081 |
| | V10 (%) | 23.10 ± 3.55 | 14.73 ± 6.37 | < 0.0001 | 12.63 ± 5.59 | < 0.0001 | 0.233 |
| **parotid** | mean dose (Gy) | 6.99 ± 0.80 | 5.91 ± 0.45 | < 0.0001 | 5.89 ± 0.78 | < 0.0001 | 0.793 |
| | V10 (%) | 16.53 ± 7.30 | 6.50 + 4.73 | < 0.0001 | 7.52 ± 5.51 | < 0.0001 | 0.339 |
| **Peritoneum** | mean dose (Gy) | 10.02 ± 0.49 | 9.54 ± 0.46 | < 0.0001 | 9.31 ± 0.46 | < 0.0001 | 0.022 |
| | V10 (%) | 39.09 ± 5.80 | 35.17 ± 4.38 | 0.002 | 30.2 ± 10.44 | 0.002 | 0.097 |

**B**

| | Primary target (18 Gy) mean ± SD (Gy) | Secondary target (12 Gy) mean ± SD (Gy) | p value |
|---|---|---|---|
| **Red marrow irradiation** | 18.49 ± 0.28 | 15.77 ± 0.78 | < 0.0001 |
| **Yellow marrow irradiation** | 18.46 ± 0.37 | 15.61 ± 1.24 | < 0.0001 |